# Framework for Modeling Coarse-Grained Soil Behavior Using 3D Printed Soil Analogs

A. Martinez & S.S. Ahmed

University of California Davis, Davis, California, USA

ABSTRACT: This paper presents the initial developments of a framework for modeling the compression behavior of coarse-grained soil using 3D printed particle analogs. This framework consists of a newly developed normalization scheme for 1-D compression response based on Hertz contact theory. The scheme normalizes the differences in stiffness of the natural and 3D printed particles' constituent materials. To explore the capabilities of the proposed framework, this paper presents results of 1D compression tests on assemblies composed of spherical particles of constituent materials with Young's moduli that span over two orders of magnitude (steel, glass and 3D printed resin). These initial results indicate that the stress-strain behavior of the assemblies can be normalized to be independent of constituent material stiffness. The presented framework can be useful for modeling the behavior of natural soil by testing representative 3D printed analogs, provided that the different aspects of the soils, such as particle shape, size, surface roughness and gradation are properly reproduced.

#### 1 INTRODUCTION

The mechanical behavior of coarse-grained soil is governed by skeletal forces transmitted through particle-particle contacts resulting from applied boundary stresses (Santamarina, 2003). The properties of the particles, such as their shape, size, surface roughness and mechanical properties of their constituent materials control the normal and shear deformation response of the contacts. These particle-scale interactions govern the global-scale response observed on element-scale tests in the lab and on a larger scale in the field.

This research provides the initial developments of a framework envisioned to unify the 1D compression stress-strain behavior of assemblies composed of particles with different constituent materials. The main aspect of this framework is a normalization scheme based on contact mechanics theory that aims to normalize the influence of constituent material stiffness. This scheme is envisioned to allow for interpretation of 1D compression response only as a function of particle and packing properties, such as particle size, shape, gradation and void ratio. As part of this initial development, the research presented herein examines the stress-strain behavior of assemblies of spheres of two well-characterized

materials (steel and borosilicate glass), and of 3D Printed (3DP) spheres.

#### 2 BACKGROUND

This section presents a brief review of previous work on contact mechanics theory and experiments, and on studies on 3DP particle analogs.

## 2.1 Elastic and Elastoplastic Contact Response

Hertz contact mechanics theory describes the normal force-displacement behavior of two elastic curved bodies in contact. Hertzian contact stress is developed when the two curved bodies come in contact and deform under the applied load. The contact stress is a function of the normal contact force, and the radii of curvature and the modulus of elasticity and Poisson's ratio of both bodies. According to Hertz theory, if two elastic spheres of radii  $R_1$  and  $R_2$  are pressed into contact with a normal force F, the contact deformation,  $\delta$ , is:

$$\delta = \left(\frac{9}{16} \frac{F^2}{RE^{*2}}\right)^{1/3} \tag{1}$$

where, *R* is the effective radius of curvature expressed as:

$$\frac{1}{R} = \frac{1}{R_1} + \frac{1}{R_2} \tag{2}$$

and,  $E^*$  is the effective Young's modulus defined as:

$$\frac{1}{E^*} = \frac{1 - v_1^2}{E_1} + \frac{1 - v_2^2}{E_2} \tag{3}$$

where  $E_1$  and  $E_2$  are the Young's moduli and  $v_1$  and  $v_2$  are the Poisson's ratios of the two bodies.

Hertz theory assumes an elastic response; however, most materials exhibit elastoplastic behavior. Previous studies indicate that the normal force-displacement response of two spherical bodies pressed against each other generally follows the behavior predicted by Hertz theory within a certain force interval. For instance, Antonyuk et al. (2005) presented four stages of the force-displacement relationship for particles tested in interplaten compression, as shown in Figure 1. The initial stage I reflects the deformation of the micro-asperities on the body's surface. Cavarretta et al. (2010) have also observed a similar initial ductile response in this stage. Ductile deformation continues until the contact normal force F exceeds the threshold load  $N_{GT}$ , which depends on the roughness of the surfaces, the curvature of the surfaces at the point of contact, and the Young's modulus of the material (Greenwood & Tripp 1967). Once F exceeds  $N_{GT}$ , the forcedisplacement response is elastic and follows Hertz theory in stage II (Figure 1). Point N in Figure 1 represents a transition between stage II and stage III, where material plastic yielding initiates and the behavior again diverges from Hertz theory. Hertzian response is thus engaged for values of F within the range  $N_{GT} < F < nN_{GT}$ , where *n* is a coefficient that depends on material properties and quantifies the upper bound of the regime where elastic deformation takes place (Cavarretta et al. 2012). At higher forces,  $F > nN_{\rm GT}$ , the displacement response diverges from the Hertz theory and permanent deformations occur, as shown in stage III of Figure 1. Stage III usually involves deformations that accumulate at a higher rate than predicted by Hertz theory due to material yielding. With further increase in force, a maximum value referred to as the 'first breakage point' is reached. At this point, the particle begins to suffer significant breakage as shown in the Stage IV.

# 2.2 Research on particle-particle contact behavior

Several researchers have studied the mechanical response of particles to identify the parameters that affect the mechanical behavior. A number of authors performed particle-particle and single particle crushing tests on different materials and reported that the force-displacement behavior undergoes a transition from approximately linear behavior at lower forces to Hertzian behavior at higher force levels (e.g. Cole & Peters 2007, 2008, Cavarretta et al. 2010, 2012, 2016). Cavarretta at al. (2010) also concluded that the threshold force at which Hertzian

behavior takes over is dependent on particle size, roundness, roughness and the Young's modulus, and proposed a new particle-scale failure criterion. Other authors (e.g. Senetakis et al. 2013) observed that stronger particles with smaller mean surface roughness show a considerably higher initial tangential stiffness compared to weaker particles with higher mean surface roughness. Nadimi & Fonseca (2017) presented a methodology to obtain 3D numerical representation of irregularly shaped grains and performed single-grain crushing tests on silica sand and stressed the importance of particle shape over surface roughness to calibrate the contact behavior of sand. Zhao et al. (2015) investigated the single-particle fracture behavior of two different types of natural sand particles using a nanofocus Xray CT and reported that the fragmentation of particles is scale invariant and depends on initial particle morphology, heterogeneity and mineralogy.

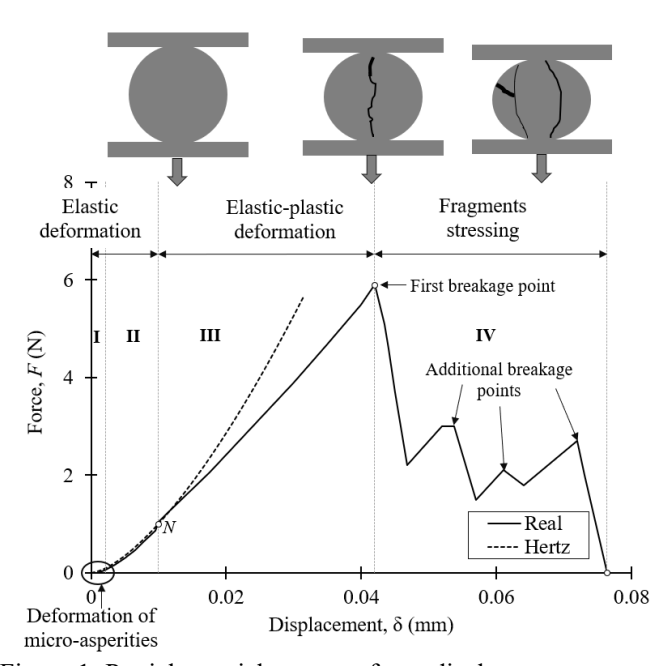


Figure 1. Particle-particle contact force-displacement curve up to failure (after Antonyuk, et al. 2005)

2.3 Previous studies on 3D printed soil analogs Rapid advances in 3D printing technology have enabled researchers to reproduce coarse-grained soil particles with independent control over particle size and shape and gradation. In recent years, several researchers have produced 3DP particles with different sizes and shapes. For example, Miskin & Jaeger (2013) used an evolutionary algorithm to find connection between particle shape mechanical response of granular materials and performed triaxial tests on assembly of 3DP spheres compare them with molecular dynamics simulations. Athanassiadis et al. (2014) conducted triaxial tests on assemblies of 3DP particles of different shapes and expressed the dependence of assembly stiffness on confining pressure by a power law  $(E \propto \sigma_{\text{con}}^n)$ , where the exponent captures the shape dependence. Hanaor et al. (2016) performed

triaxial tests on 3DP particles of different shapes and sizes and demonstrated that 3DP analogs can qualitatively reproduce soil behavior, including the effect of particle shape. Matsumura et al. (2017) reproduced bonded gravel specimen by means of X-ray imaging and 3D printing and performed triaxial tests on the 3DP specimens. They reported the observation of both stress-level dependency and volumetric dilatancy typical of frictional granular materials during triaxial compression testing.

These studies have demonstrated the usefulness and potential of 3DP particle analogs. The objective of the research presented herein is to provide means to qualitatively reproduce the mechanical behavior of natural soils using 3DP analogs.

# 3 PROPOSED NORMALIZATION FRAMEWORK

The current research is focused on the force-displacement response of particles in contact within the Hertzian behavior range (i.e. stage II in Figure 1 within the range  $N_{\rm GT} < F < nN_{\rm GT}$ ). The applied boundary stresses that control the contact normal forces between particles were carefully selected to avoid significant yielding at contacts and particle breakage. As the response of the contacts is elastic within this range, the principal mechanical property of interest is the particles' Young's modulus (i.e. normal stiffness).

The average normal force F at particle-particle contacts within a random packing of equal size spheres is related to the applied effective boundary stress  $\sigma$ , the particle radius R and the assembly void ratio. This relationship can be expressed as

$$F = C\sigma R^2 \tag{4}$$

where, C is a coefficient that depends on void ratio e, and is expressed as  $C = \pi(1+e)^2/3$  (Santamarina 2003). Considering spheres of equal sizes in an assembly of particles with boundary stress  $\sigma$ , Eq. 1 can be written as:

$$\delta = \left[ \frac{9}{16} \frac{(C \sigma R^2)^2}{R E^{*2}} \right]^{1/3} \tag{5}$$

For a contacts within assemblies of mono-sized spheres with the same void ratio and particle size but composed of particles of different materials (i.e. with different Young's modulus) to undergo the same deformation (i.e.  $\delta_1 = \delta_2$ ) the following condition must be met:

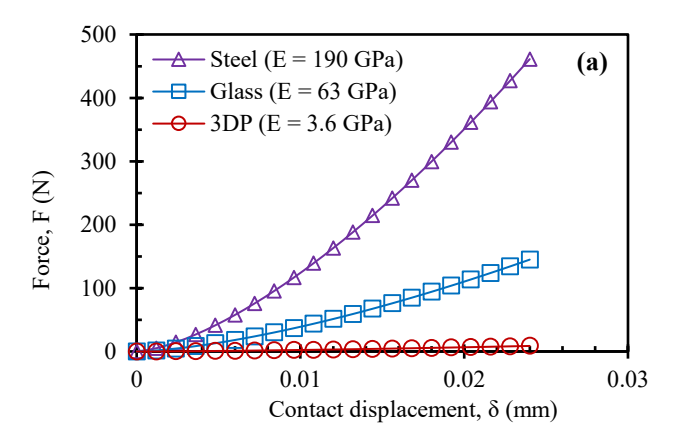
$$\left[\frac{9}{16} \frac{\left(C\sigma_1 R^2\right)^2}{RE_1^{*2}}\right]^{1/3} = \left[\frac{9}{16} \frac{\left(C\sigma_2 R^2\right)^2}{RE_2^{*2}}\right]^{1/3} \tag{6}$$

From which the following relationship is obtained:

$$\frac{\sigma_1}{E_1^*} = \frac{\sigma_2}{E_2^*} \quad or \quad \frac{F_1}{E_1^*} = \frac{F_2}{E_2^*}$$
 (7)

This relationship, obtained from Hertz theory, indicates that the same deformation will be experienced at the particle-particle contacts as long as the ratio of the applied boundary stress (or contact force) to material Young's modulus is equal for the two assemblies composed of different materials.

The Hertzian force-deformation relationship for contacts between particles composed of three different materials are plotted in Figure 2a. The curves correspond to equal sized spheres with a radius of 1.588 mm pressed against each other. As shown in Figure 2a, higher force is required to obtain a given deformation for contacts between particles with higher Young's modulus. In contrast, Figure 2b presents curves for the same materials in terms of normalized force ( $F/E^*$ ). The three curves overlap, indicating that the normalized force required to produce a given contact deformation is independent of material Young's modulus.



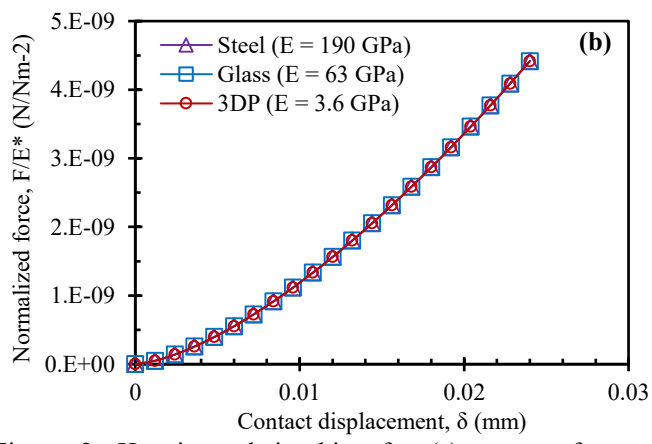


Figure 2. Hertzian relationships for (a) contact force vs. displacement, and (b) normalized contact force vs. displacement for steel, glass and 3DP particle contacts.

# 4 MATERIALS AND METHODS FOR EXPERIMENTS

# 4.1 Materials used for the experiments

Three different materials were tested in this study: steel, borosilicate glass, and 3DP particles. Various properties of the materials are listed in Table 1.

Table 1: Properties of materials used in experiments

Material	Young's modulus, E (GPa)	Poisson ratio, v	Specific gravity, $G_{\rm s}$
Steel	190	0.30	7.82
Borosilicate glass	63	0.20	2.23
3DP Resin	3.6	0.30	1.15

## 4.2 Test equipment

# 4.2.1 3D printer and printing of analogs

Form 2 from Formlabs was used to print the 3DP particle analogs. This printed utilizes stereolithography technology. A resin tank with a transparent bottom holds liquid photo-polymerizing resin. A laser is used to selectively illuminate the resin to cure and solidify thin layers. This process is repeated to create layers of 25 microns in thickness. Utilizing this resolution, a single spherical particle with a diameter of 3.175 mm is printed in 127 layers. Particles are printed in batches of 360 using clear resin (FLGPCL02 from Formlabs).

After printing, the spheres are transferred to an alcohol bath where they are held for 10 minutes to remove residual uncured resin. Then, the printed spheres are post-cured for two hours in a chamber that exposes them to ultraviolet light at a temperature of 150°C. The post-curing process further enhances the resin's mechanical properties.

### 4.2.2 1D compression test setup

A schematic of the experimental setup is shown in Figure 3. A custom-made compression mold made of 316 stainless steel with inside diameter and height of 63.5 mm contains the specimen. A GeoJac digital load actuator is used to apply strain-controlled compression to the specimen during testing. Displacement is measured with a linear variable differential transformer (LVDT), and the applied load is measured with a load cell. Larger forces were applied to the steel specimen, followed by those applied to the glass specimen, and the 3DP specimen was tested under the lowest force. To achieve acceptable data resolution, the steel, glass and 3DP specimens were tested with 8.90 kN, 2.22 kN, and 0.44 kN load cells, respectively.

## 4.2.3 Test plan and specimen preparation

Specimens of three different materials were tested, as shown in Table 3. The specimens were composed of monosized spherical particles with a diameter of 3.175 mm. The specimens were prepared by pouring the spheres in the testing mold in three lifts. The side of the specimen was tapped with a rubber mallet to densify it to its target void ratio. Specimens of each material were prepared at two different initial void ratios, 0.55±0.025 and 0.60±0.025. The maximum normal stress applied to the specimens composed of

different materials was selected carefully to prevent breakage or significant deformation of the particles.

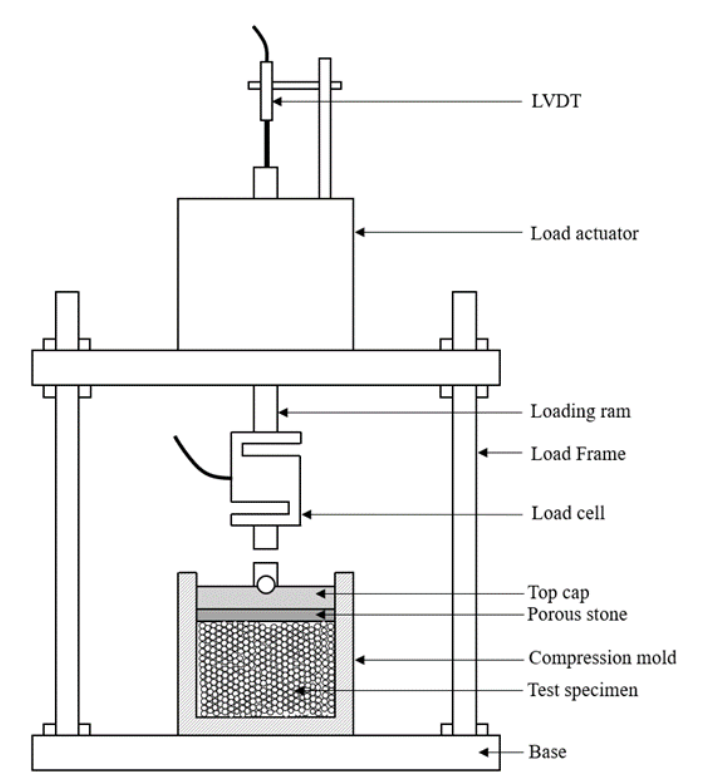


Figure 3. Schematic of 1D compression test

#### 5 RESULTS AND DISCUSSION

The results of 1D compression tests in terms of  $\Delta e$  vs.  $\sigma$  performed on specimens with void ratios of 0.55±0.025 and 0.60±0.025 are presented in Figures 4a and 5a, respectively. As expected, specimens composed of particles with constituent materials with higher Young's modulus require higher stress for a certain change in void ratio to be achieved (Figures 4a and 5a). The compression response of specimens of the three materials, in terms of normalized stress ( $\sigma/E^*$ ), aggregate into a tighter band (Figures 4b and 5b), showing that the normalization scheme accounts for some of the differences in response. However, in normalized space the curve for the 3DP particles specimen lies to the right of steel and glass specimens.

In contrast to the analytical relationships presented in Figure 2b, the experimental results on assemblies indicate that the proposed framework does not completely normalize the effect of particle stiffness. This was expected as the proposed framework does not address other effects that influence the compression behavior of granular assemblies, such as particle rearrangement and resulting fabric changes.

Figures 4c and 5c present the results using a different normalization scheme, one that normalizes the applied stress by the Young's modulus raised an empirically-determined power n = 0.75 as:

$$\frac{\sigma_1}{E_1^{*n}} = \frac{\sigma_2}{E_2^{*n}} \tag{8}$$

As shown, the compression curves seem to collapse to a single relationship, indicating that a power normalization better captures effects than the purely analytical scheme (Eq. 7). Such effects are likely to be related to rearrangement of particles, as previously described, to plastic deformations of

micro-asperities at small loads, and possibly yielding at a small number of contacts due to concentration of forces, as shown by Discrete Element Modeling (DEM) simulations by authors such as Barreto Gonzalez (2009).

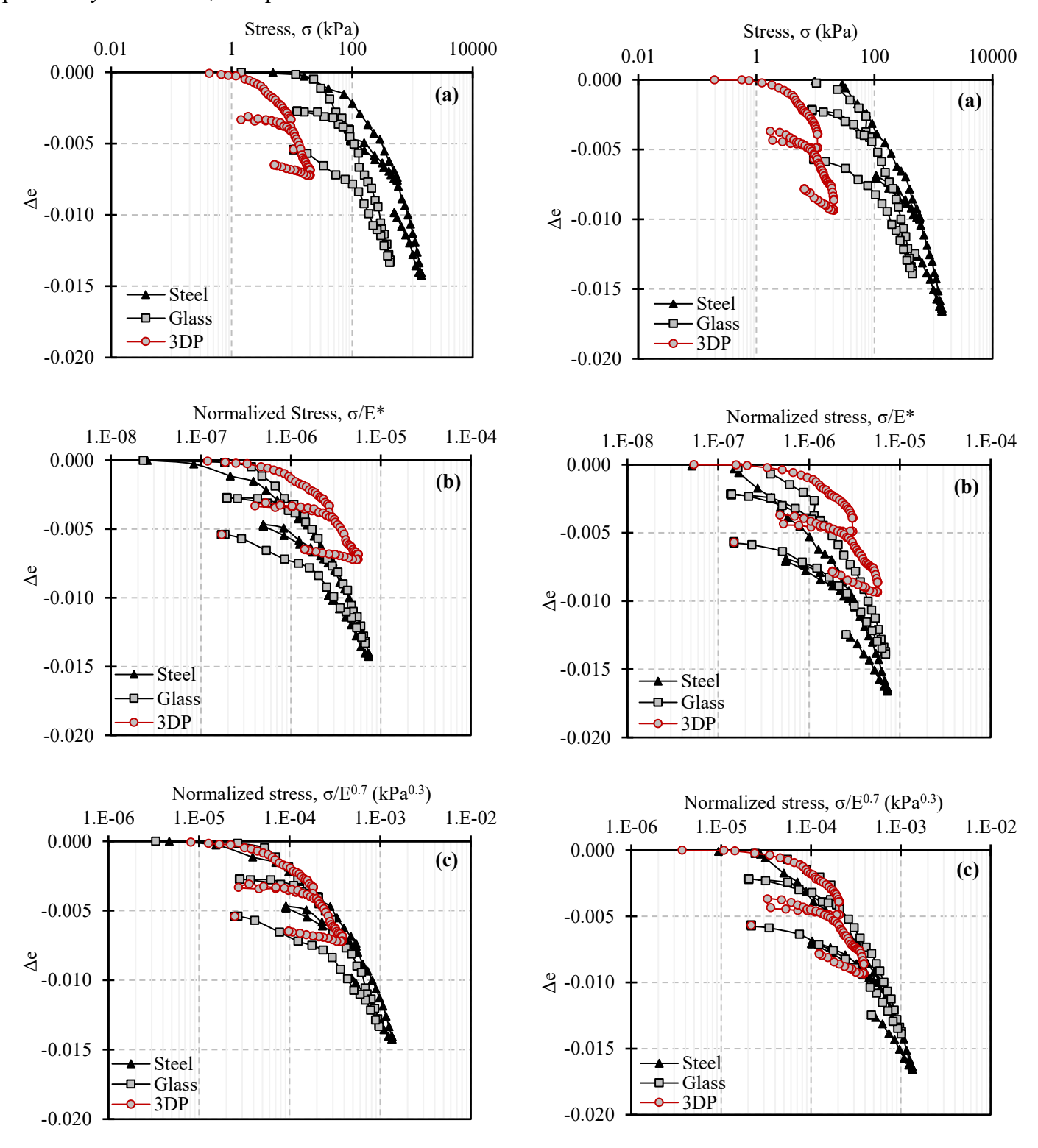


Figure 4. (a)  $\Delta e$  vs. stress, (b)  $\Delta e$  vs. normalized stress ( $\sigma/E^*$ ), and (c)  $\Delta e$  vs. normalized stress ( $\sigma/E^{*n}$ ) plots for initial void ratio of  $0.55\pm0.025$ 

Figure 5. (a)  $\Delta e$  vs. stress, (b)  $\Delta e$  vs. normalized stress ( $\sigma/E^*$ ), and (c)  $\Delta e$  vs. normalized stress ( $\sigma/E^*$ n) plots for initial void ratio of  $0.60\pm0.025$ 

Figure 6 presents values for the slope of the compression curves for normalized stress values larger than  $2x10^{-4}$  kPa<sup>0.3</sup> (from Figures 4c and 5c).

Although there is some scatter, the results imply that that the slope of the compression curves is independent of Young's modulus. However, the slope values are influenced by the void ratio, with the larger values for specimens with higher void ratio. This trend is likely due to more pronounced particle rearrangement and higher concentration of forces on contacts on specimens with higher void ratios.

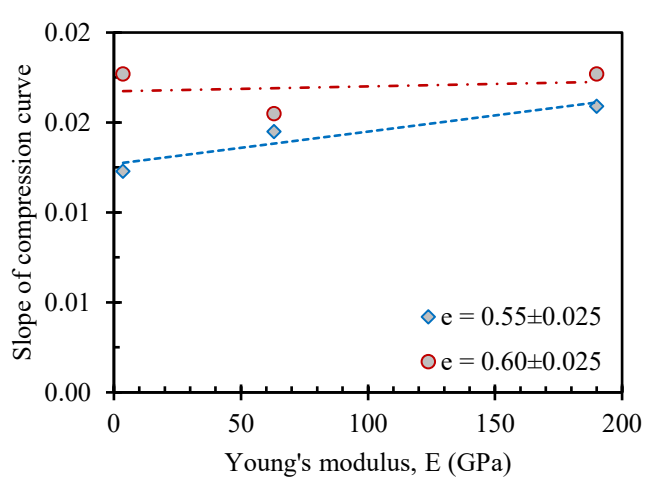


Figure 6. Plot of  $C_c$  vs. E for different void ratios

The results presented in Figures 4, 5 and 6 provide evidence that the 1D compression behavior of specimens composed particles of a given material (i.e. steel, glass) can be modeled in normalized space using 3DP particle analogs. However, it is noted that the results presented herein pertain to specimens composed of mono-sized spherical particles, and do not address the potential effects of differences in particle surface roughness. The applicability of the proposed framework should be further evaluated on assemblies composed of natural soil particles and 3DP particle analogs with faithfully reproduced particle shapes and sizes.

#### 6 CONCLUSION

This paper presents the initial developments of a framework aimed at normalizing the effect of constituent material Young's modulus on the mechanical response of granular assemblies. 1D compression tests on assemblies of 3D printed, steel and glass spheres were performed, and two different normalizations were presented. One normalization scheme is purely analytical and uses Hertz contact mechanics, while and the second scheme is semiempirical. The initial results presented herein indicate that the compression behavior of the specimens collapses to a unique relationship if an empirical exponent is utilized in the normalization. However, the influence of material, particle and packing properties on the value of this exponent should be further studied. The results presented herein provide evidence of the potential of the proposed framework and normalization scheme to allow for modeling of behavior of coarse grained soils using 3D printed particle analogs.

#### 7 ACKNOWLEDGEMENTS

The research was funded by National Science Foundation (NSF) project number 1735732. This support is greatly acknowledged.

#### 8 REFERENCES

- Antonyuk, S., Tomas, J., Heinrich, S. & Mörl, L. 2005. Breakage behaviour of spherical granulates by compression. *Chemical Engineering Science*, 60(14): 4031-4044.
- Athanassiadis, A.G., Miskin, M.Z., Kaplan, P., Rodenberg, N., Lee, S.H., Merritt, J., Brown, E., Amend, J., Lipson, H. & Jaeger, H.M. 2014. Particle shape effects on the stress response of granular packings. *Soft Matter*, 10(1): 48-59.
- Barreto Gonzalez, D. (2009). Numerical and experimental investigation into the behaviour of granular materials under generalized stress states. PhD thesis, Department of Civil and Environmental Engineering, Imperial College London.
- Cavarretta, I., Coop, M. & O'Sullivan, C. 2010. The influence of particle characteristics on the behaviour of coarse grained soils. *Géotechnique*, 60(6): 413-423.
- Cavarretta, I., O'Sullivan, C. & Coop, M.R. 2016. The relevance of roundness to the crushing strength of granular materials. *Géotechnique*, 67(4): 301-312.
- Cavarretta, I., O'Sullivan, C., Ibraim, E., Lings, M., Hamlin, S. & Wood, D.M. 2012. Characterization of artificial spherical particles for DEM validation studies. *Particuology*, 10(2): 209-220.
- Cole, D.M. & Peters, J.F. 2007. A physically based approach to granular media mechanics: grain-scale experiments, initial results and implications to numerical modeling. *Granular Matter*, 9(5): 309-321.
- Cole, D.M. & Peters, J.F. 2008. Grain-scale mechanics of geologic materials and lunar simulants under normal loading. *Granular Matter*, 10(3): 171-185.
- Greenwood, J.A. & Tripp, J.H. 1967. The elastic contact of rough spheres. *Journal of Applied Mechanics*, 34(1): 153-
- Hanaor, A.H., Gan, Y., Revay, M., Airey, D.W. & Einav, I. 2016. 3D printable geomaterials. *Géotechnique*, 66(4): 323-332
- Matsumura, S., Kobayashi, T., Mizutani, T. & Bathurst, R.J. 2017. Manufacture of Bonded Granular Soil Using X-Ray CT Scanning and 3D Printing. Geotechnical Testing Journal, 40(6): 1000-1010.
- Miskin, M.Z. & Jaeger, H.M. 2013. Adapting granular materials through artificial evolution. *Nature Materials*, 12(4): 326-331.
- Nadimi, S. & Fonseca, J. 2017. Single-Grain Virtualization for Contact Behavior Analysis on Sand. *Journal of Geotechnical and Geoenvironmental Engineering*, 143(9), 06017010.
- Santamarina, J.C. 2003. Soil behavior at the microscale: Particle forces. *Proc., Soil Behavior and Soft Ground Construction*, GSP No. 119, ASCE, Reston, VA, 25-56.
- Senetakis, K., Coop, M.R. & Todisco, M.C. 2013. Tangential load–deflection behaviour at the contacts of soil particles. *Géotechnique Letters*, 3(2): 59-66.
- Zhao, B., Wang, J., Coop, M.R., Viggiani, G. & Jiang, M. 2015. An investigation of single sand particle fracture using X-ray micro-tomography. *Géotechnique*, 65(8): 625-641.